Analysis of Magnetotelluric Transfer Functions to Determine the Usefulness of ZTEM Data in the Nechako Basin, South-Central British Columbia (Parts of NTS 092O, N, 093B, C, F, G)

J.E. Spratt, Geophysical Consultant, Wakefield, QC, jessicaspratt@sympatico.ca

C.G. Farquharson, Memorial University of Newfoundland, St. John's, NL

J.A. Craven, Natural Resources Canada, Geological Survey of Canada–Central Canada, Ottawa, ON

Spratt, J.E., Farquharson, C.G. and Craven, J.A. (2012): Analysis of magnetotelluric transfer functions to determine the usefulness of ZTEM data in the Nechako Basin, south-central British Columbia (parts of NTS 092O, N, 093B, C, F, G); *in* Geoscience BC Summary of Activities 2011, Geoscience BC, Report 2012-1, p. 151–162.

Introduction

As part of Geoscience BC's initiative to develop the potential for hydrocarbon resources in central British Columbia (BC), several geological and geophysical projects have been undertaken within the Nechako Basin, including a high-density broadband and audio-magnetotelluric survey. The Nechako Basin is an Upper Cretaceous to Oligocene sedimentary basin located in the interior plateau of BC between the Coastal Mountains and the Rocky Mountains (Figure 1). The potential for reservoir sands has been noted in the Cretaceous sedimentary packages of the basin (Hannigan et al., 1994; Riddell, 2006); however, these packages are extensively overlain by variable thicknesses of Eocene and Neogene volcanics, as well as Quaternary and glacial deposits, thus limiting the surficial exposure of the sediments and interfering with interpretations of the subsurface structure. Magnetotelluric (MT) data collected within the Nechako Basin in 2007 were used successfully to image the conductivity structure beneath two-dimensional (2-D) profiles and show that the method can differentiate between varying rock types and identify structural features in the subsurface (Spratt and Craven, 2011).

It has been suggested that acquiring airborne z-axis tipper electromagnetic (ZTEM) data over the Nechako Basin could be useful for mapping the thickness of overlying volcanic layers and identifying areas of reservoir potential, particularly in the regions between the MT profiles where the conductivity structure is unknown. The ZTEM method measures airborne electromagnetic data that provide information on the 3-D conductivity structure of the shallow subsurface. It is a cost-effective way to record tipper data, calculated from the vertical component of the magnetic field, over a broad region with a high-density sampling distribution; however, the data are not sensitive to 1-D layers (Holtham and Oldenburg, 2010), and limitations on the frequencies measured may result in low resolution of the models and shallow penetration depths. As MT data record the horizontal and vertical components of magnetic field, along with the electric fields, the tipper data are available at each recorded site. Transfer functions from measured MT data, as well as synthetic data calculated from the existing 2-D conductivity models, have been analyzed to determine which features could be resolved with additional airborne ZTEM data.

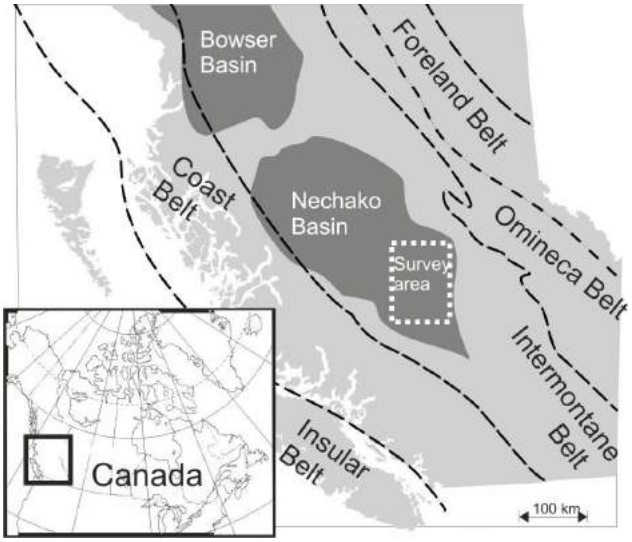

Figure 1. Location of the Nechako Basin and the magnetotelluric survey area.

Keywords: Nechako Basin, magnetotellurics, ZTEM, hydrocarbon exploration, electromagnetics

This publication is also available, free of charge, as colour digital files in Adobe Acrobat® PDF format from the Geoscience BC website: http://www.geosciencebc.com/s/DataReleases.asp.

Geological and Geophysical Background

Geological Setting

A series of Mesozoic and Cenozoic clastic basins formed within the Intermontane Belt of the Canadian Cordillera in response to oceanic and island-arc terrane amalgamation along the western edge of ancestral North America (Mon-

ger et al., 1972, 1982; Gabrielse and Yorath, 1991). Postaccretionary sedimentary and volcanic sequences are preserved in the study area within the Nechako Basin. These are underlain by the Carboniferous to Early Cretaceous Stikine island-arc terrane and the Permian to Middle Triassic oceanic Cache Creek terrane. Extension during the Eocene resulted in magmatism, regional transcurrent faulting and volcanism (Price, 1994; Struik and MacIntyre, 2001). Volcanism during the Miocene and Pliocene produced the mafic volcanic rocks that blanket much of the region (Mathews, 1989; Andrews and Russell, 2007).

The Nechako Basin is up to 5 km thick and consists of three primary geological elements: Early Cretaceous clastic marine and fluvial rocks of the Taylor Creek and Skeena groups, Eocene volcaniclastic rocks that include the Endako and Ootsa Lake groups, and Neogene Chilcotin Group basalts (Figure 2). The Taylor Creek and Skeena groups in the study area are composed of interbedded chert, pebble conglomerate, sandstone, siltstone and shale (Riddell, 2006). The Endako Group comprises andesitic to basaltic volcanic flows, tuff, breccia and minor amounts of sedimentary rocks (Riddell, 2006), whereas the Ootsa Lake Group has intermediate to felsic flows and a higher amount of sedimentary material (Riddell, 2006, 2011). The near-horizontal basaltic flows of the Chilcotin Group blanket portions of the region with an average thickness of <20 m, reaching up to 200 m in localized paleochannels (Andrews and Russell, 2008; Andrews et al., 2011).

Geophysical Investigations

Several geological and geophysical surveys have been undertaken to ascertain the distribution of Cretaceous rocks, which are the most prospective for oil and gas. Since the 1960s, several exploration wells drilled through the Nechako Basin by Canadian Hunter Exploration Limited, Esso, Honolulu Oil Corporation Limited and Hudson's Bay Oil and Gas Company Limited (shown on Figure 2) have provided stratigraphic information and borehole logs of petrophysical properties (Hannigan et al., 1994; Riddell et al., 2007; Smith, 2007). Analysis of this information indicated that reservoir-quality rock was only present in Cretaceous sedimentary packages, primarily the Taylor Creek and

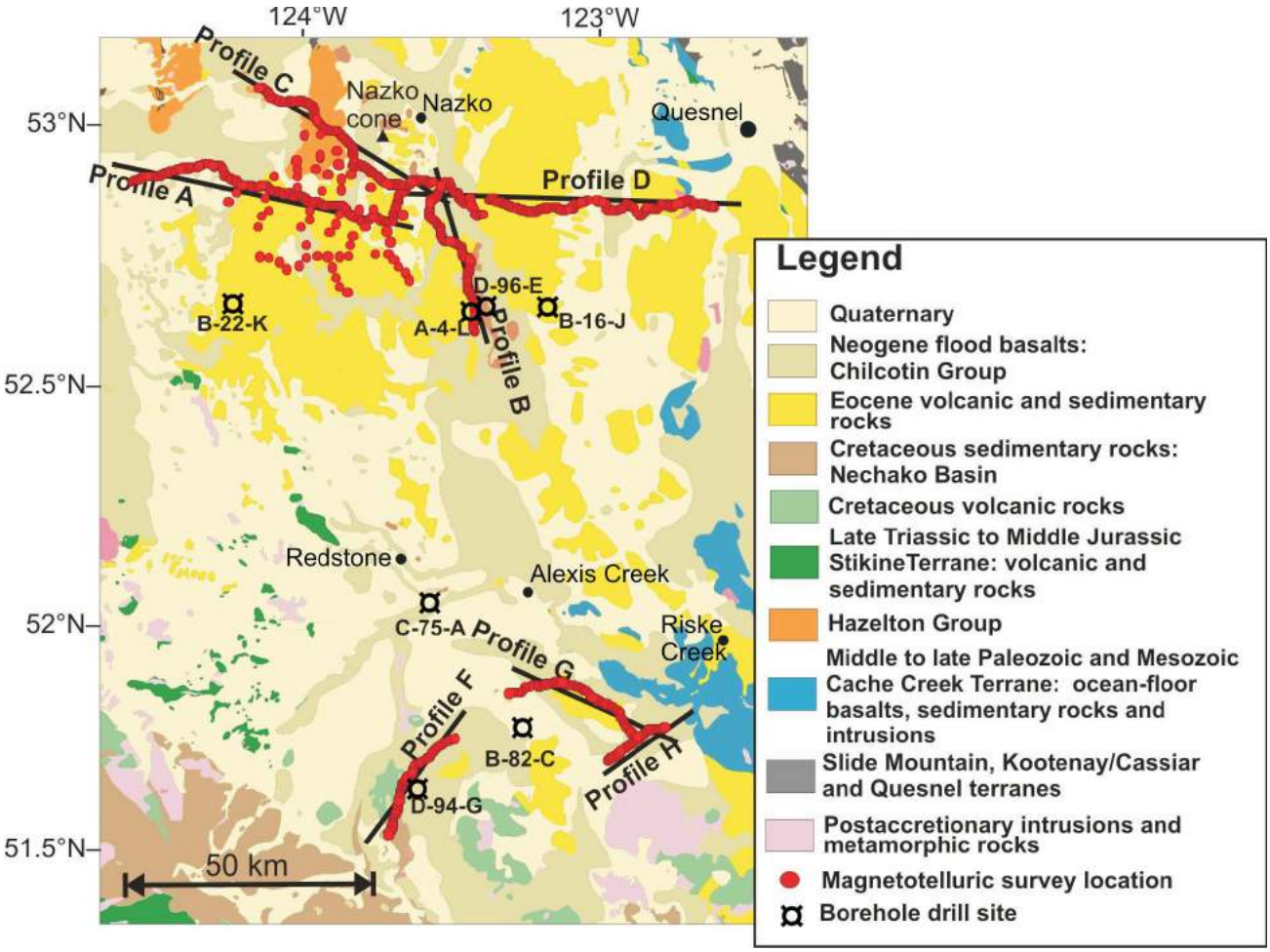

Figure 2. Detailed geology of the study area, showing the location of the magnetotelluric survey sites and the two-dimensional profile traces (modified from Riddell, 2006).

Skeena groups (Riddell et al., 2007). Interpretations of early 1980s Canadian Hunter gravity and seismic data, as well as new seismic data collected by Geoscience BC in 2008, suggest that the sedimentary packages are located in separate sub-basins rather than one larger basin (Hayward and Calvert, 2008; Calvert at al., 2011). This implies that the units with hydrocarbon potential may not regionally underlie the extensive volcanic cover. Locating the regional extent of Cretaceous sedimentary rocks is therefore crucial in developing an understanding of this potential. The presence of near-surface volcanic rocks significantly complicates the interpretation of some geophysical methods.

Overview of Magnetotelluric Results

The magnetotelluric (MT) method provides information on the present-day, in situ electrical conductivity of the subsurface by measuring natural time-varying electromagnetic fields at the Earth's surface (e.g., Jones, 1992). The MT method involves comparison of the horizontal components of the electric and magnetic fields of the Earth, measured at the surface. These are related to each other by a 2 by 2 complex impedance tensor that varies as a function of frequency and position of observation (Wait, 1962). The vertical magnetic field is also recorded and is related to the horizontal magnetic components by the geomagnetic-transfer function (TF). The depth of penetration of the fields is dependent on frequency (i.e., the lower the frequency the greater the depth) and the resistivity of the material (i.e., the greater the resistivity, the greater the depth; Cagniard, 1953). The transverse electric (TE) and transverse magnetic (TM) modes of electromagnetic (EM)–field propagation refer to the directions parallel and perpendicular to geoelectric strike, respectively. Modelling the vertical field-transfer functions, typically displayed as induction vectors that point towards current concentrations in the Earth, can identify conductors in the subsurface.

In the fall of 2007, combined high-frequency audio-magnetotelluric (AMT) and broadband magnetotelluric (BBMT) data were collected at a total of 734 sites through the southern part of the Nechako Basin at a site spacing of <500 m (Figure 2; Spratt and Craven, 2009). The data were processed by Geosystem Canada using robust remote-reference techniques that generally resulted, in excellent data quality covering a range of nearly seven period decades (orders of magnitude) from 0.0001 to 1000 s (Spratt and Craven, 2009). The dataset was divided into seven separate profiles for analysis and subsequent inversions. Each site was analyzed for distortion, dimensionality and directionality, and a 2-D model was generated along each profile by inverting data from the TM-, TE- and TF-mode data (Spratt and Craven, 2010, 2011).

Results of 2-D modelling of the TE-mode, TM-mode and vertical-field transfer-function (HZ) components of the MT data indicate that the method can differentiate between varying rock types and reveal structure in the subsurface (Figure 3; Spratt and Craven, 2011). The 2-D MT models generated along the profiles, in general, reveal three distinct horizontal units that characterize the conductivity structure of the Nechako Basin; these units are best resolved in the models along profiles A, B, C and F (Figure 3). A near-surface resistive layer (>500 Ω·m) is interpreted as the Chilcotin basalts, which blanket portions of the region to depths of <50 m but can locally thicken up to 200 m in paleochannels. A low-resistivity unit underlying the near-surface resistor varies in thickness between 0 and 4000 m, and appears to have two end members with varying resistivity signatures. The Cretaceous sedimentary units are characterized by moderate resistivities (10–100 Ω·m) that are laterally highly variable, whereas lower, more uniform conductivity values (<4 Ω·m) appear to be associated with the Eocene volcaniclastic groups. The base of the Nechako Basin is marked by an increase in resistivity (>200 Ω·m) associated with the deeper underlying Cretaceous volcanic units or island-arc terranes. In addition to the layered resistivity structure, the data also image folding and faulting of the Nechako sediments, structural features that may provide an environment for trapping hydrocarbons.

Transfer-Function Data

ZTEM Method

Similar to the MT method, ZTEM uses natural fields as the source of transmitted energy to resolve a conductivity-depth profile of the Earth. The method involves interpretation of transfer functions that relate the local airborne vertical field to mutually perpendicular horizontal magnetic fields recorded at a reference station on the ground. Common line spacings used in airborne ZTEM surveys are 100–400 m (e.g., Geotech Limited, 2009; Lo et al., 2009; Sattel et al., 2010), data are recorded at an output sampling rate of 2.5 samples/second and the recording equipment is typically flown at a speed of 80 km/h for a nominal sample spacing of 8 m along each line flown (e.g., Holtham and Oldenburg, 2010). In theory, current ZTEM instrumentation can measure data in the frequency range 22–2800 Hz; however, typical surveys process data at 30, 45, 90, 180, 360 and occasionally 720 Hz (e.g., Geotech Limited, 2009; Lo et al. 2009).

The MT skin depth of the magnetic fields can be a useful guide in estimating the penetration depths of the fields at specific periods. In a uniform half space, it is given by

$$d = 503(\rho T)^{1/2},$$

where d is the depth in metres, ρ is the resistivity value and T is the period (Cagniard, 1953). At the longest ZTEM period (0.033 s), we would expect penetration depths (and model resolution) of approximately 2 km in the Chilcotin

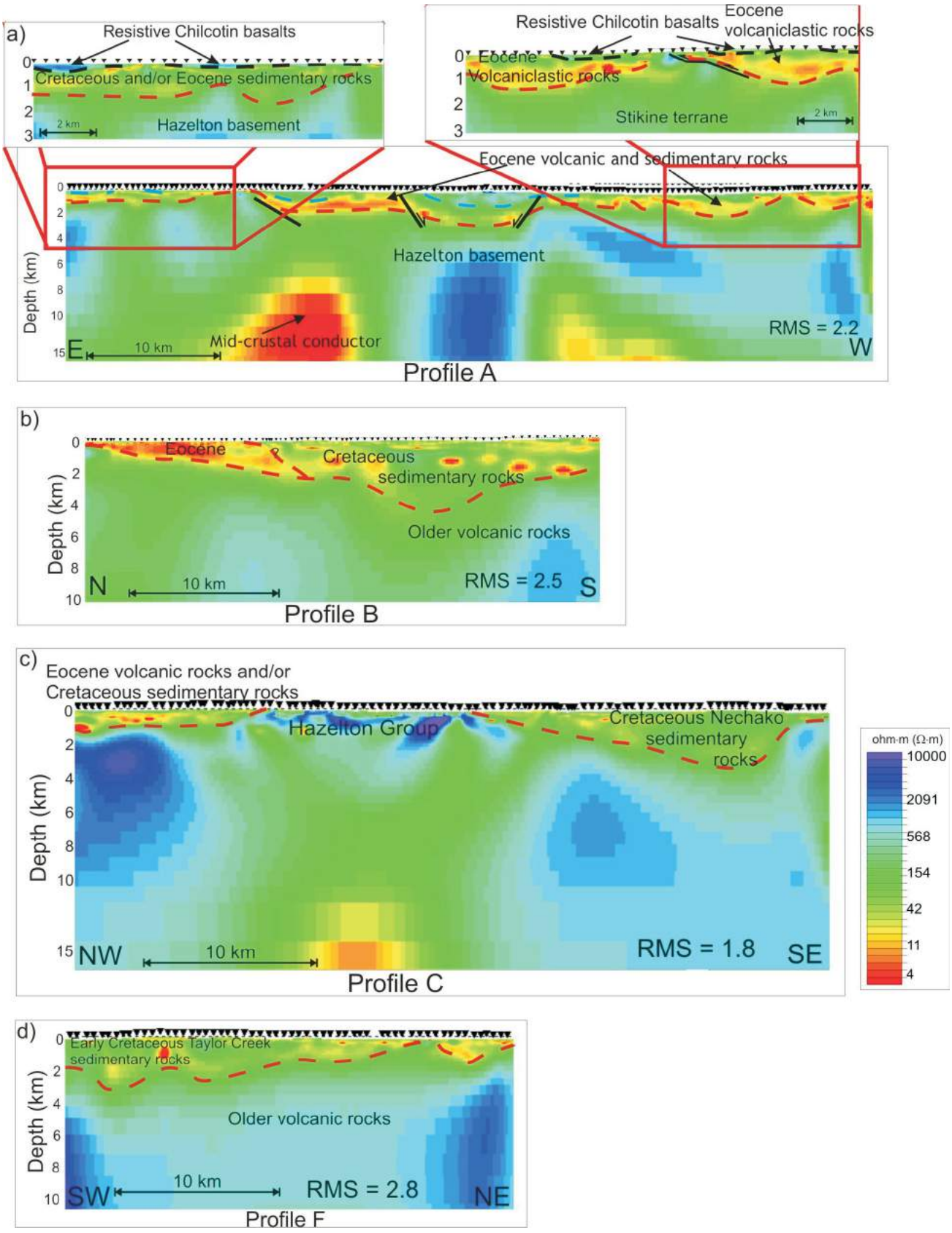

Figure 3. Two-dimensional conductivity models and interpretations for **a)** profile A, **b)** profile B, **c)** profile C, and **d)** profile F. The red dashed line illustrates the interpreted base of the Nechako Basin and the black lines represent faults.

Group (>500 Ω·m), 900 m in the Cretaceous groups (10–100 Ω·m) and 200 m in the Eocene group (<4 Ω·m), where the units are sufficiently thick. This suggests that the method may be capable of differentiating between different rock types at shallow depths but will not be able to image the base of the basin.

For every three successive sites during acquisition the Nechako Basin MT data in 2007 (Figure 4), the vertical-

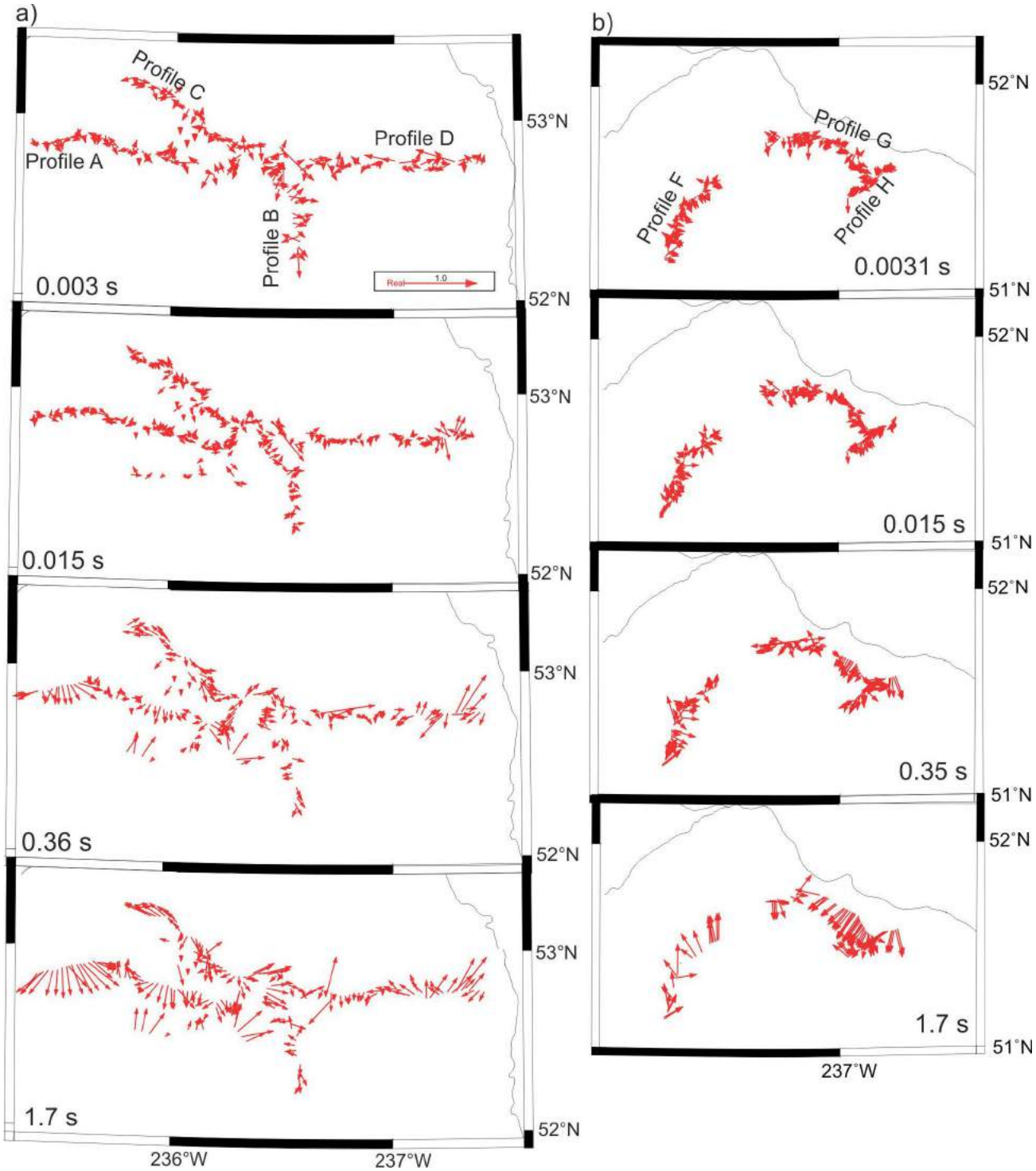

Figure 4. Induction vectors from transfer functions of measured vertical-field magnetotelluric data at periods of 0.003, 0.015, 0.36 and 1.7 s, showing data from the northern **(a)** and southern **(b)** portions of the survey area. The arrows point towards conductors with a magnitude of less than 1.

field data were recorded in the BBMT range (200–0.0001 Hz) at the first site (Figure 5a) and the AMT range (10 000–1 Hz) at the second site (Figure 5e), and no vertical-field data were recorded at the third site (Figure 4). In general, the data quality is excellent to periods below 1 s (Figure 5a, e). Figure 5 shows examples of different fre-

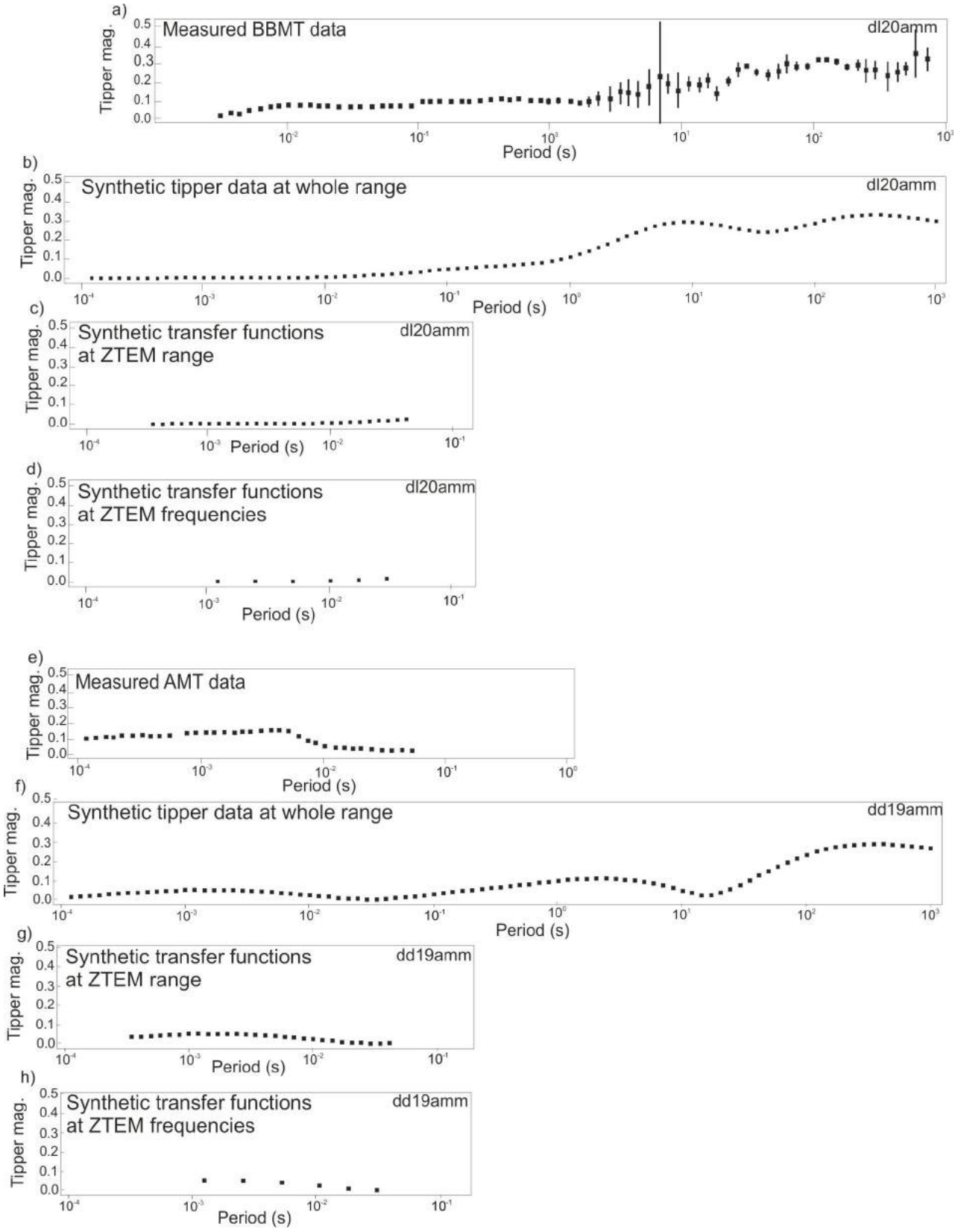

quency ranges used in various 2-D model inversions for two sites: one located above conductive Eocene volcaniclastic rocks (Figure 5a–d) and the other located above exposed Cretaceous sedimentary units (Figure 5e–h).

Deriving Synthetic Data

Synthetic transfer-function data have been computed from the 2-D conductivity models produced by the inversion of all components of the MT data using the GEOSYSTEM SRL WinGlink® MT interpretation software package (Figures 5b, f). The data have been computed at a site spacing of 100 m along each of the MT profiles, a site spacing that reaches the limit of the modelling program. These synthetic data have been generated by creating additional sites along the profiles, importing the final 2-D models, running a forward inversion and then saving the calculated responses as station data. Note that no noise was added to the synthetic data. New models were then generated along the profiles using these synthetic data and various frequency ranges: the entire frequency range (0.001–10 000 Hz, Figure 5b, f), the frequency range of the ZTEM data (22–2800 Hz, Figure 5c, 5h), and the specific frequencies used in the ZTEM surveys (Figure 5d, 5h).

Two-Dimensional Modelling

Several 2-D conductivity models have been generated, using the WinGlink® interpretation software package, along the main MT profiles. More than 200 iterations have been employed in the inversion for each model, using either the measured or the synthetic transfer-function data at various frequencies. Examples of the data used in the various models are shown in Figure 5. Each inversion was initiated with a uniform half space of 500 Ω·m as a starting model. The inversions of measured data used a smoothing value (tau) of 3, a Tyz absolute data-error floor of 0.01 and existing data errors. Each inversion of synthetic data used a tau of 3, a Tyz absolute data-error floor of 0.001 and a standard deviation error of 1%.

Two-dimensional inversions were carried out on the measured 2007 MT magnetic-transfer functions (e.g., Figure 5a, e). The results of these inversions serve as a bench mark against which the results obtained from the synthetic ZTEM data can be measured. The subset of the measured vertical-field MT data that corresponds to the frequency range appropriate for ZTEM surveys has been modelled to show what can be obtained from ZTEM data were they to be collected along the MT profiles, and under the best possible conditions. The synthetic transfer-function data have been inverted using data in the MT measurable frequency range (0.001–10000 Hz; Figure 5b, f), in the ZTEM measurable range (22–2800 Hz; Figure 5c, g) and at the six frequencies specific to typical ZTEM analysis (30, 45, 90, 180, 360, 720 Hz; Figure 5d, h).

Figure 5. Plots of the tipper magnitude for two sites at the various frequency distributions included in inversions: **a)** measured data from broadband-magnetotelluric (BBMT) site dd22amm, located above the conductive Eocene volcaniclastic rocks; **b)** synthetic data derived from the 2-D magnetotelluric (MT) model at site dd22amm; **c)** synthetic data at site dd22amm, over the z-axis tipper electromagnetic (ZTEM) period range; **d)** synthetic data at site dd22amm, at the periods typically analyzed using the ZTEM method; **e)** measured data from high-frequency audio-magnetotelluric (AMT) site dl19aam, located above exposed Cretaceous sedimentary rocks; **f)** synthetic data derived from the 2-D MT model at site dl19aam; **g)** synthetic data at site dl19aam, over the ZTEM period range; and **h)** synthetic data at site dl19aam, at the periods typically analyzed using the ZTEM method.

Results and Conclusion

Results of the 2-D modelling of profiles A, B, C, and F are presented in Figures 6–9. For each profile, the original 2-D model derived from all three components of the data measured and at each MT site location over the entire measured frequency range are shown (Figures 6a, 7a, 8a, 9a). Also shown are models derived using only the HZ component of the measured data over the entire frequency range (Figures 6c, 7b, 8b, 9b); models derived from the HZ component of the measured data at the recordable ZTEM frequency range (Figures 6d, 7c, 8c, 9c); and models generated using only the HZ component of the synthetic data over the entire frequency range (Figures 6e, 7d, 8d, 9d), at the recordable ZTEM frequency range (Figures 6f, 7e, 8e, 9e) and at the specific frequency used in ZTEM surveys (Figure 6g, 7f, 8f, 9f).

In order to test the modelling parameters applied, an additional model was generated along profile A by inverting all three components of the synthetic MT data (TM-mode, TE-mode and transfer-function HZ data; Figure 6b). When compared to the original 2-D model, the synthetic data show good resolution of the subsurface-conductivity structure, indicating that the modelling program and selected parameters are capable of generating an accurate image of the subsurface-conductivity structure. Modelling of the transfer functions from measured MT data alone does not appear to resolve the subsurface-conductivity structure along any of the profiles, regardless of the frequency range that was inverted (Figures 6c, 6d, 7b, 7c, 8b, 8c, 9b, 9c). This may be due to inherent errors associated with real data and, if so, it should be noted that we expect the airborne data to have higher errors. It could also be a result of the large station spacing compared to airborne ZTEM surveys. Along profile A, synthetic data were modelled at the measured station spacing for comparison with those modelled at a spacing of 100 m. Additionally, a model was generated for a small section at the easternmost end of profile A using synthetic data at a site spacing of 25 m. Although the resulting model was much smoother, the structural resolution was not improved with a higher station density.

Along profile A (Figure 6), the conductivity structure is not well resolved using the synthetic HZ data over the entire frequency range (Figure 6e) when compared to the original 2-D model. Models of the synthetic HZ data using frequencies limited to the ZTEM range, however, reveal features that are similar to the original 2-D model, resulting in reasonable conductivity values to appropriate depths and significant structural detail (Figure 6f). This resolution is lost when further limiting the frequencies to the six ZTEM frequencies (Figure 6g).

In comparison to the original 2-D model along profile B (Figure 7a), inversion of the synthetic data over the entire frequency range reveals the general subsurface-conductivity structure, including the highly conductive Eocene volcaniclastic rocks at the north end of the profile and the laterally variable and moderate conductivities of the Cretaceous sediments over the southern half of the profile, and it shows an appropriate basin depth beneath the entire profile (Figure 7d). Results using both the ZTEM range and the six specific ZTEM frequencies show the highly conductive Eocene units, but these are only observed to depths of <200 m (Figure 7e, f). The Cretaceous sedimentary rocks are imaged as laterally variable and moderately conductive in the ZTEM-based model (Figure 7f), consistent with the key signature observed in the original MT data–based models (Figure 7a); however, the overall structure and specific conductivity variations within this unit are significantly different from the original 2-D model.

Results along profile C are illustrated in Figure 8. These show that the synthetic data resolve well the resistive Hazelton Group units to reasonable depths of 2–3 km, regardless of the frequency distribution that is inverted (Figure 8d–f). The lateral continuity of the moderate conductivities at the southeastern end of the profile, interpreted as Cretaceous sedimentary rocks, is broken but the conductivity values are significantly lower (<4 Ω·m), closer to those of the Eocene groups. In addition, the overall structure or distribution of conductivity variations is different from that of the original 2-D model, particularly when using the six ZTEM frequencies (Figure 8f). The moderate conductivities at the northwestern end of the profile were interpreted as Eocene and/or Cretaceous groups in the original 2-D model because the conductivity signature was difficult to classify (Figure 8a). Although the synthetic data inverted over the ZTEM range image this feature reasonably well, the model including just the six ZTEM frequencies shows a laterally uniform, highly conductive unit that would be interpreted as Eocene volcaniclastic rocks (Figure 8f).

Figure 9 shows the results for profile F. Here, consistent with borehole lithology, the original 2-D model revealed

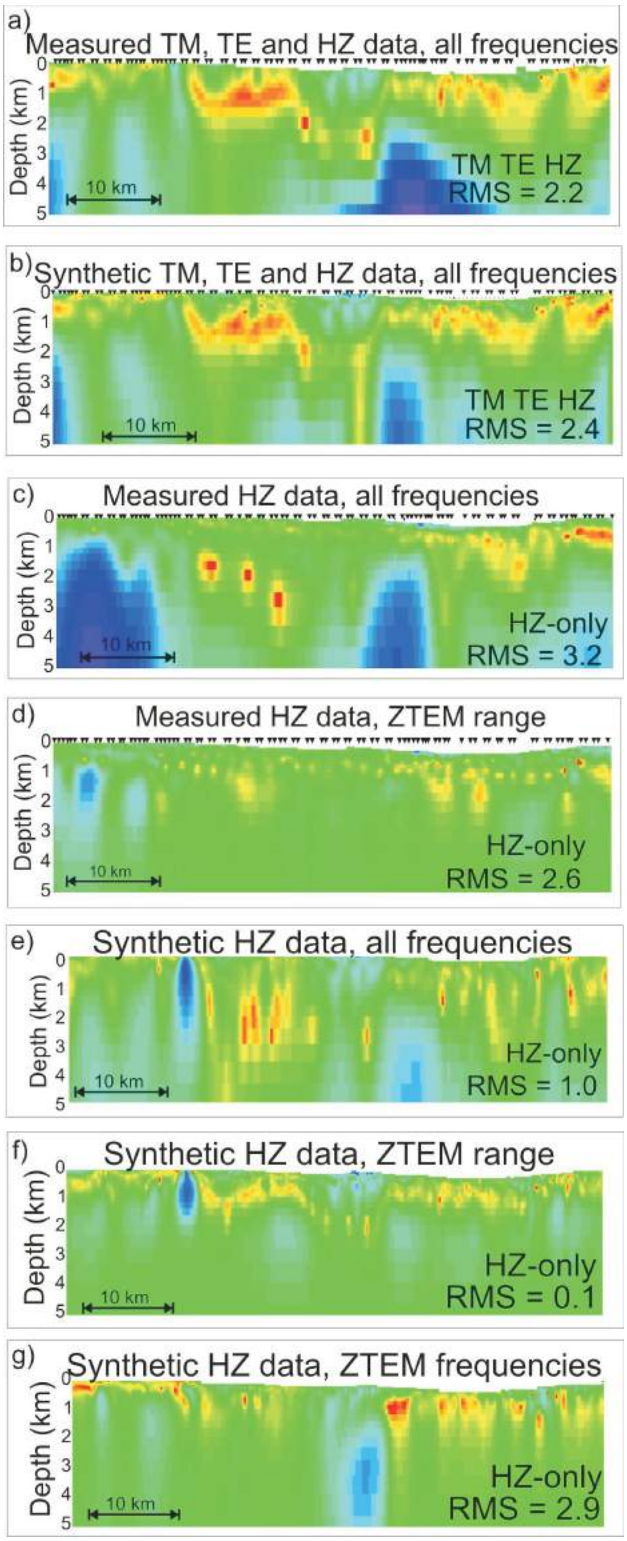

Figure 6. Results of two-dimensional (2-D) modelling of measured and synthetic MT data along profile A: **a)** original 2-D model derived from all components of the measured MT data (equivalent to upper 5 km of Figure 3); **b)** model of all components of the synthetic data over the seven-decade frequency range; **c)** model of the measured HZ data over the seven-decade frequency range; **d)** model of the measured HZ data over the ZTEM frequency range; **e)** model of the synthetic HZ data over the seven-decade frequency range; **f)** model of the synthetic HZ data over the ZTEM frequency range; and **g)** model of the synthetic data at the six specific ZTEM frequencies.

Cretaceous Taylor Creek sedimentary rocks to depths of 2–3 km (Figure 9a). Inversion of the synthetic HZ data shows laterally variable conductivities, the values being slightly lower but comparable to those associated with Cretaceous sedimentary rocks. The general structure, distribution of the conductivity variations and depth of the units, however, are not well resolved, particularly when using just the six ZTEM frequencies (Figure 9f).

Inversions of synthetic data indicate that modelling the transfer-function data alone can give a reasonable image of the conductivity structure of the subsurface; however, revealing specific features at depth is highly dependent on the frequencies included in the inversion. In ideal geological terranes, where the depth to target, conductivity value and structure are suitable (e.g., imaging moderate conductivities at depths of <1 km), the ZTEM method may be very useful in determining the conductivity structure. Within the Nechako Basin, where the thickness of units, conductivity values and lateral structure are highly variable, the method may be capable of identifying the conductive Eocene volcaniclastic rocks to shallow depths but incapable of differentiating between the Eocene groups and the Cretaceous sedimentary rocks. It is hoped that this work will serve as a guide to the circumstances under which ZTEM surveys will be most useful in identifying the stratigraphic units and structures of interest to mineral or hydrocarbon exploration. Future work includes synthesizing the results of the remaining three profiles.

Acknowledgments

This work was supported by Geoscience BC. The authors thank M. Pilkington for his rapid review of this manuscript.

Natural Resources Canada, Earth Science Sector contribution 20110267.

References

Andrews, G.D.M. and Russell, J.K. (2007): Mineral exploration potential beneath the Chilcotin Group, south-central BC: preliminary insights from volcanic facies analysis; *in* Geological Fieldwork 2006, Geoscience BC, Report 2007-1, p. 229–238, URL <http://www.empr.gov.bc.ca/Mining/Geoscience/PublicationsCatalogue/Fieldwork/Documents/22-Andrews.pdf> [November 2011].

Andrews, G.D.M. and Russell, J.K. (2008): Cover thickness across the southern Interior Plateau, British Columbia (NTS 092O, P, 093A, B, C, F): constraints from water-well records; *in* Geoscience BC Summary of Activities 2007, Geoscience BC, Report 2008-1, p. 11–20, URL <http://www.geosciencebc.com/i/pdf/SummaryofActivities2007/SoA2007-Andrews_original.pdf> [November 2011].

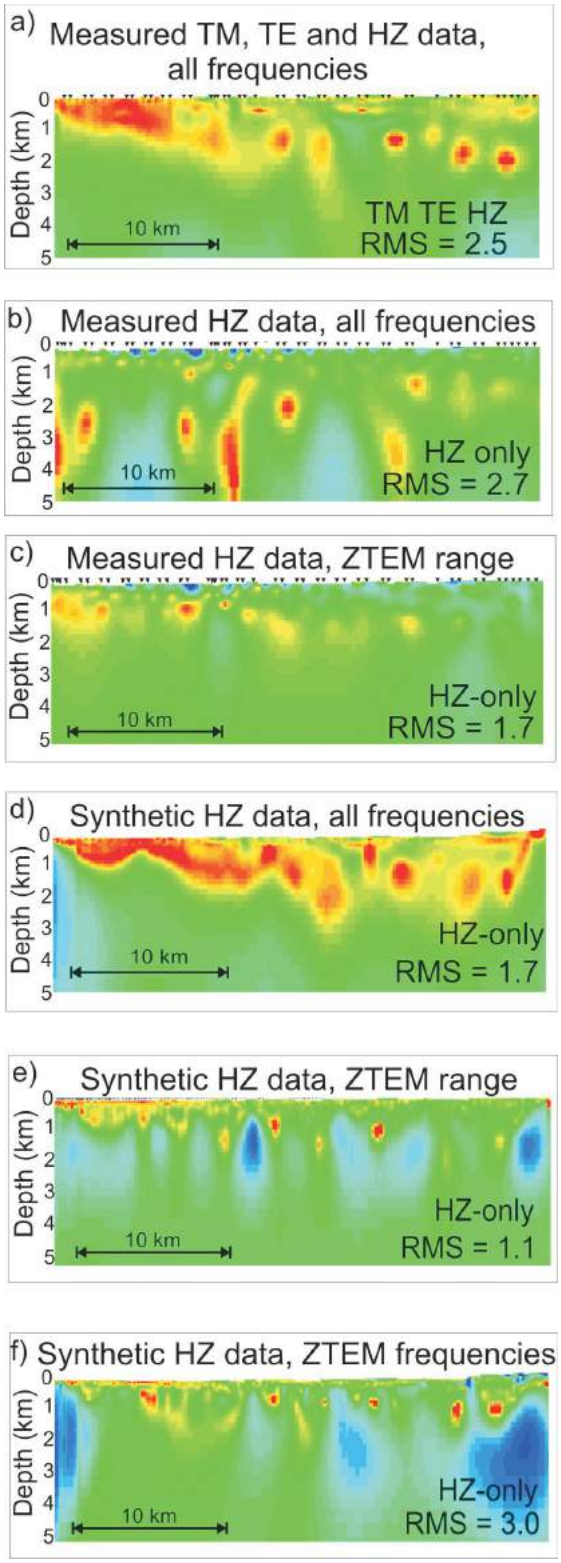

Figure 7. Results of two-dimensional (2-D) modelling of measured and synthetic MT data along profile B: **a)** original 2-D model derived from all components of the measured MT data; **b)** model of the measured HZ data over the seven-decade frequency range; **c)** model of the measured HZ data over the ZTEM frequency range; **d)** model of the synthetic HZ data over the seven-decade frequency range; **e)** model of the synthetic HZ data over the ZTEM frequency range; and **f)** model of the synthetic HZ data at the six specific ZTEM frequencies.

Andrews, G.D.M., Plouffe, A., Ferbey, T., Russell, J.K., Brown, S.R. and Anderson, R.G. (2011): The thickness of Neogene and Quaternary cover across the central Interior Plateau, British Columbia: analysis of water-well drill records and implications for mineral exploration potential; Canadian Journal of Earth Sciences, v. 48, no. 6, p. 973–986.

Cagniard, L. (1953): Basic theory of the magnetotelluric method of geophysical prospecting; Geophysics, v. 18, p. 605–635.

Calvert, A.J., Hayward, N.E., Spratt, J.E. and Craven, J.A. (2011): Seismic reflection constraints on upper crustal structures in the volcanic-covered central Nechako basin, British Columbia; Canadian Journal of Earth Sciences, v. 48, no. 6, p. 1021–1037.

Gabrielse, H. and Yorath, C.J. (1991): Tectonic synthesis; *in* Geology of the Cordilleran Orogen in Canada, H. Gabrielse and C.J. Yorath (ed.), Geological Survey of Canada, Geology of Canada, no. 4, p. 677–705 (also Geological Society of America, Geology of North America, v. G-2).

Geotech Limited (2009): Helicopter-borne z-axis tipper electromagnetic (ZTEM) and aeromagnetic survey, Mt. Milligan test block; Geoscience BC, Report 2009-7, 51 p., URL <http://www.geosciencebc.com/s/2009-07.asp> [November 2011]

Hannigan, P., Lee, P.J., Osadetz, K.J., Dietrich, J.R. and Olsen-Heise, K. (1994): Oil and gas resource potential of the Nechako-Chilcotin area of British Columbia; BC Ministry of Energy and Mines, GeoFile 2001-6, 5 maps at 1:1 000 000 scale, URL <http://www.empr.gov.bc.ca/Mining/Geoscience/PublicationsCatalogue/GeoFiles/Pages/2001-6.aspx> [November 2011].

Hayward, N. and Calvert, A.J. (2008): Structure of the southeastern Nechako Basin, south-central British Columbia (NTS 092N, O; 093 B, C): preliminary results of seismic interpretation and first-arrival tomographic modelling; *in* Geoscience BC Summary of Activities 2007, Geoscience BC, Report 2008-1, p. 129–134, URL <http://www.geosciencebc.com/i/pdf/SummaryofActivities2007/SoA2007-Hayward_original.pdf> [November 2011].

Holtham, E. and Oldenburg, W. (2010): Three-dimensional inversion of ZTEM data; Geophysical Journal International, v. 182, p. 168–192, doi:10.1111/j.1365-246X.2010.0463.x

Jones, A.G. (1992): Electrical conductivity of the continental lower crust; *in* Continental Lower Crust, D.M. Fountain, R.J. Arculus and R.W. Kay (ed.), Elsevier, Amsterdam, The Netherlands, p. 81–143.

Lo, B., Legault, J., Kuzmin, P. and Fisk, K. (2009): Advances in airborne EM: introducing ZTEM; South African Geophysical Association (SAGA), 11th Biennial Technical Meeting and Exhibition, extended abstracts, p. 101–104.

Mathews, W.H. (1989): Neogene Chilcotin basalts in south-central British Columbia: geology, ages, and geomorphic history; Canadian Journal of Earth Sciences, v. 26, p. 969–982.

Monger, J.W.H., Price, R.A. and Templeman-Kluit, D. (1982): Tectonic accretion of two major metamorphic and plutonic welts in the Canadian Cordillera; Geology, v. 10, p. 70–75.

Monger, J.W.H., Souther, J.G. and Gabrielse, H. (1972): Evolution of the Canadian Cordillera—a plate tectonic model; American Journal of Science, v. 272, p. 577–602.

Price, R.A. (1994): Cordilleran tectonics in the evolution of the Western Canada Sedimentary Basin; *in* Geological Atlas of the Western Canada Sedimentary Basin, G.D. Mossop and I.

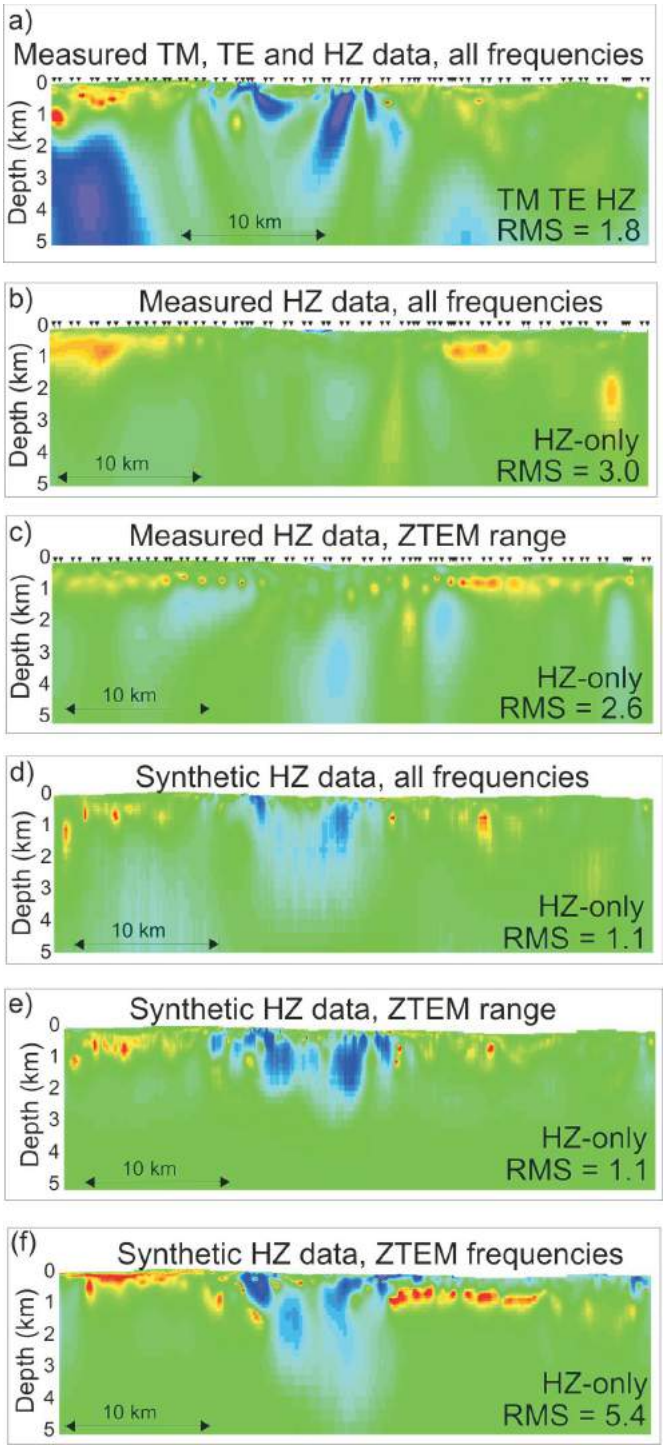

Figure 8. Results of two-dimensional (2-D) modelling of measured and synthetic MT data along profile C: **a)** original 2-D model derived from all components of the measured MT data; **b)** model of the measured HZ data over the seven-decade frequency range; **c)** model of the measured HZ data over the ZTEM frequency range; **d)** model of the synthetic HZ data over the seven-decade frequency range; **e)** model of the synthetic HZ data over the ZTEM frequency range; and **f)** model of the synthetic HZ data at the six specific ZTEM frequencies.

Shetsen (comp.), Canadian Society of Petroleum Geologists and Alberta Research Council, 510 p., URL <http://www.ags.gov.ab.ca/publications/wcsb_atlas/atlas.html> [November 2011].

Riddell, J.M., comp. (2006): Geology of the southern Nechako Basin, NTS 92N, 92O, 93B, 93C, 93F, 93G; BC Ministry of Energy and Mines, Petroleum Geology Map 2006-1, 3 sheets at 1:400 000 scale.

Riddell, J. (2011): Lithostratigraphic and tectonic framework of Jurassic and Cretaceous intermontane sedimentary basins of south-central British Columbia; Canadian Journal of Earth Sciences, v. 48, no. 6, p. 870–896.

Riddell, J., Ferri, F., Sweet, A. and O'Sullivan, P. (2007): New geoscience data from the Nechako Basin project; *in* Nechako Initiative Geoscience Update 2007, BC Ministry of Energy and Mines, Petroleum Geology Open File 2007-1, URL <http://www.empr.gov.bc.ca/Mining/Geoscience/PublicationsCatalogue/OilGas/OpenFiles/Pages/PGOF2007-1.aspx> [November 2011].

Sattel, D., Witherly, K. and Becken, M. (2010): A brief analysis of ZTEM data from the Forrestanian test site, WA; Australian Society of Exploration Geophysicists (ASEG), Extended Abstracts, v. 2010, no. 1, p. 1–4.

Smith, I.F. (2007): Petrophysical analysis—Nechako Basin; *in* Nechako Initiative Geoscience Update 2007, BC Ministry of Energy and Mines, Petroleum Geology Open File 2007-1, URL <http://www.empr.gov.bc.ca/Mining/Geoscience/PublicationsCatalogue/OilGas/OpenFiles/Pages/PGOF2007-1.aspx> [November 2011].

Spratt, J.E. and Craven, J.A. (2009): Preliminary images of the conductivity structure of the Nechako Basin, south-central British Columbia (NTS 092N, O, 093B, C, F, G) from magnetotelluric methods; *in* Geoscience BC Summary of Activities 2008, Geoscience BC, Report 2009-1, URL <http://www.geosciencebc.com/i/pdf/SummaryofActivities2008/SoA2008-Spratt_original.pdf> [November 2011].

Spratt, J.E. and Craven, J. (2010): Magnetotelluric imaging of the Nechako Basin, British Columbia, Canada; Geological Survey of Canada, Current Research, 2010-3, 12 p., URL <http://geopub.nrcan.gc.ca/moreinfo_e.php?id=261488> [November 2011].

Spratt, J. and Craven, J. (2011): Near-surface and crustal-scale images of the Nechako basin, British Columbia, Canada, from magnetotelluric investigations; Canadian Journal of Earth Sciences, v. 48. p. 987–999.

Struik, L.C. and MacIntyre, D.G. (2001): Introduction to the special issue of Canadian Journal of Earth Sciences: The Nechako NATMAP Project of the central Canadian Cordillera; Canadian Journal of Earth Sciences, v. 38, p. 485–494.

Wait, J.R. (1962): Theory of magnetotelluric fields; Journal of Research of the National Bureau of Standards, Part D: Radio Properties, v. 66d, p. 509–541.

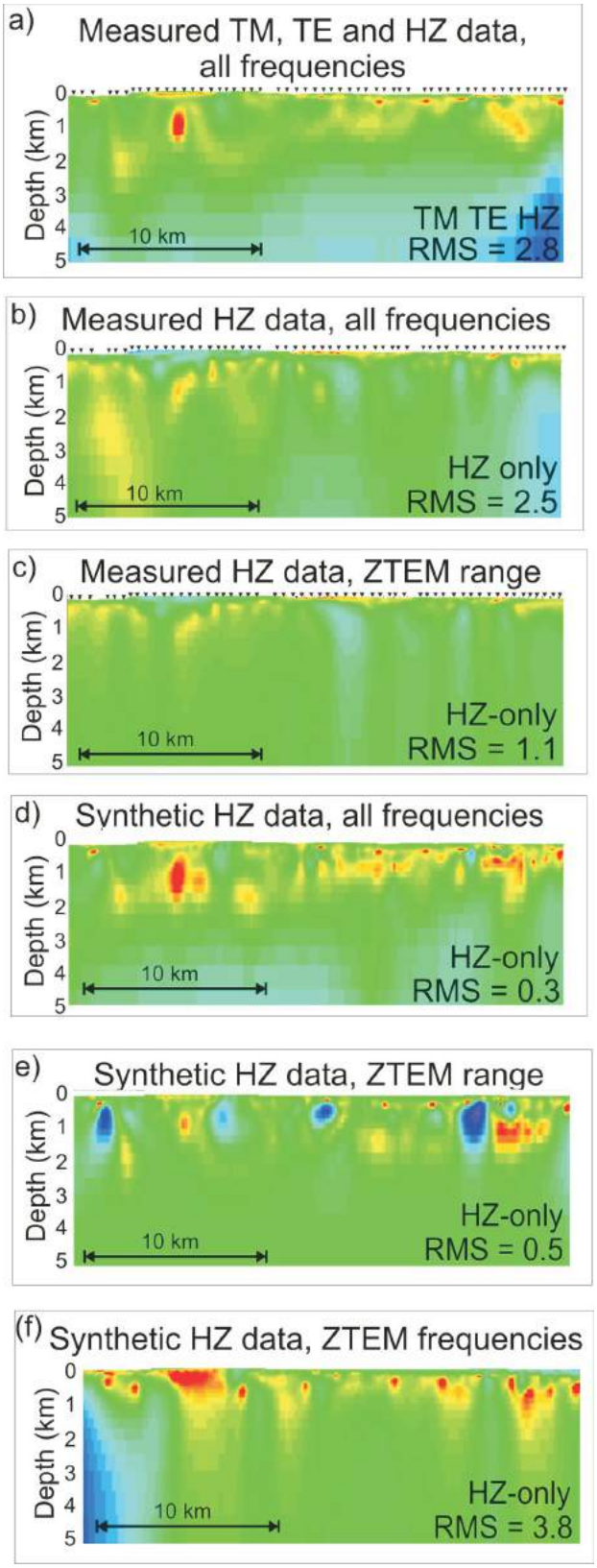

Figure 9. Results of two-dimensional (2-D) modelling of measured and synthetic MT data along profile F: **a)** original 2-D model derived from all components of the measured MT data; **b)** model of the measured HZ data over the seven-decade frequency range; **c)** model of the measured HZ data over the ZTEM frequency range; **d)** model of the synthetic HZ data over the seven-decade frequency range; **e)** model of the synthetic HZ data over the ZTEM frequency range; and **f)** model of the synthetic HZ data at the six specific ZTEM frequencies.